The Response of the Surface Circulation of the Arabian Sea to Monsoonal Forcing

L. M. BEAL

Rosenstiel School of Marine and Atmospheric Science, University of Miami, Miami, Florida

V. HORMANN

Scripps Institution of Oceanography, University of California San Diego, La Jolla, California

R. LUMPKIN AND G. R. FOLTZ

NOAA/Atlantic Oceanographic and Meteorological Laboratory, Miami, Florida

(Manuscript received 13 February 2013, in final form 3 June 2013)

ABSTRACT

Two decades of drifter and satellite data allow the authors to describe the seasonal evolution of the surface circulation of the Arabian Sea, which reverses annually with the Indian monsoon winds. This study finds several features that advance current understanding. Most significantly, northward flow appears along the length of the western boundary, together with a weak anticyclone at 6°N (a precursor to the Great Whirl) as early as March or April, one or two months before the southwest monsoon winds. This circulation is driven by planetary waves, which are initiated by wind curl forcing during the previous southwest monsoon, leading the authors to speculate that there is an oceanic mechanism through which one monsoon may precondition the next. Second, the authors find that the eastward South Equatorial Counter Current (SECC) is present year-round, fed by the northward East African Coastal Current (EACC). During the southwest monsoon the EACC overshoots the equator and splits, feeding both northward into the Somali Current and eastward into the SECC by looping back across the equator. This retroflection of the EACC is what was previously known as the southern gyre. At the surface, this circulation is obscured by strong, locally wind-driven, cross-equatorial transport. The semiannual variability of the SECC is governed by Ekman pumping over the equatorial gyre. Finally, there is broad, strong eastward flow at the mouth of the Gulf of Aden throughout the southwest monsoon, coincident with alongshore winds and a switch in sign of the wind stress curl along the axis of the atmospheric monsoon jet.

1. Introduction

The Arabian Sea is a unique region of the ocean, where the circulation switches direction annually under the influence of strong monsoon winds. During the boreal summer, or southwest monsoon, the northward advection of Southern Hemisphere waters along the western boundary, together with strong coastal upwelling, offshore flow, and mechanical wind mixing, all affect sea surface temperature (SST) (Lee et al. 2000). SST, in turn, feeds back on the winds (Vecchi et al. 2004) and on rainfall over India (Izumo et al. 2008). Hence, understanding these elements, and other basics of the circulation, is important. However, describing the monsoon circulation is challenging because large amounts of data are required in both space and time to resolve the evolution of the flow in a region with no steady circulation.

In the past, three coordinated observing efforts (1960s: International Indian Ocean Expedition; 1970s: Indian Ocean Experiment; and 1990s: World Ocean Circulation Experiment/Joint Global Ocean Flux Study) have been undertaken in the Arabian Sea, largely focusing on the southwest monsoon circulation and the western boundary. These, together with several model studies, ultimately led to the comprehensive review of Schott and McCreary (2001) and accompanying schematics of the summer and winter monsoon circulations (Schott et al. 2009). In the intervening ten or fifteen years, piracy has prevented further ship measurements, but satellite and

Corresponding author address: Lisa Beal, Rosenstiel School of Marine and Atmospheric Science, University of Miami, 4600 Rickenbacker Causeway, Miami, FL 33149.
E-mail: lbeal@rsmas.miami.edu

DOI: 10.1175/JPO-D-13-033.1

drifter data have come to maturity and can provide a robust means to go beyond these static schematics and examine the seasonally evolving surface circulation.

There have been several previous analyses specifically making use of satellite and drifter data in the Arabian Sea. Molinari et al. (1990) compiled surface-drifting buoy trajectories from 1975 to 1987 to find two counterrotating gyres in the tropical Indian Ocean during the winter or northeast monsoon: a clockwise gyre bounded by the South Equatorial Current (SEC) at 20°S and by the South Equatorial Counter Current (SECC) at about 5°S, and a counterclockwise gyre bounded by the SECC in the south and by the North Monsoon Current (NMC) at 5°N. These gyres are fed by a confluence of boundary currents along the African coast. Shenoi et al. (1999) used an expanded drifter dataset (1976–98) to show monthly-mean absolute currents and their harmonics. Most notably, they show that the eastward SECC breaks down during the summer monsoon, but that the drifter trajectories are not represented by the mean dynamic topography at this time. Although they do not highlight this result, it shows the importance of Ekman flow in the region of the SECC during the summer monsoon and we will expand on this in our study.

Annual Rossby waves are a significant feature in the Arabian Sea, dominating patterns of sea surface height (SSH) variability, particularly during the intermonsoon periods. This means that remote forcing on the evolving surface circulation could be significant in spring and fall. Brandt et al. (2002) show that the westward propagation of first- and second-mode annual Rossby waves explain 87% of the seasonal, midbasin hydrographic variance below 100 m, along 8°N. We will show that the effect of annual Rossby waves on surface currents is significant in spring, between the winter and summer monsoons.

Here, we expand on these studies by examining wind, current, and dynamic height fields of the Arabian Sea on a monthly basis. Monthly means allow us to describe the response of annual and semiannual currents to the changing winds and to track the advection of Rossby waves and other features from the east. Both the absolute flow, from a drifter climatology, and the geostrophic flow, from a drifter–altimeter synthesis, are examined. The influence of local versus remote (in time and space) forcing mechanisms is discussed.

2. Data

We use satellite scatterometer data to calculate monthly-mean winds and wind stress curl over the Arabian Sea. A seasonal climatology of absolute near-surface currents is derived from the global array of satellite-tracked drifting buoys, to provide monthly-mean maps of the circulation, together with formal error velocities. In addition, a drifter–altimeter synthesis (1993–2010) is used to map the leading modes of variance of the flow and to illustrate the monthly evolution of the geostrophic currents and the absolute dynamic topography field.

The global drifter array (Niiler 2001) became fully realized in September 2005, with 1250 drifters worldwide. There have been a total of 421 unique drifters in the Arabian Sea since then, and a median of 8 drifters each day. Each drifter consists of a surface float, with a satellite transmitter and temperature sensor, tethered to a holey sock drogue centered at 15-m depth, which minimizes slip associated with direct wind forcing (Niiler et al. 1995). The drifter follows the flow integrated over the drogue depth. Drogue status is diagnosed and only drifters with a drogue intact are used in this study (Lumpkin et al. 2013). Daily winds from the National Centers for Environmental Prediction (NCEP)–National Center for Atmospheric Research (NCAR) reanalysis, version 2, are used to estimate and remove any remaining slip (Pazan and Niiler 2000). Wind stress and the local Coriolis parameter are used to estimate the Ekman component of the flow (Ralph and Niiler 1999; Niiler 2001). All velocities are low passed at 5 days to remove tides and inertial motions. To derive monthly composites, the observations are decomposed into time-mean, annual, and semiannual amplitudes and phases to mitigate time aliasing of the mean fields caused by inhomogeneous sampling. These components are then calculated in elliptical bins, including their regression components onto first- and second-order spatial polynomials, and a term proportional to a five-month low-passed Southern Oscillation index. For more details of this methodology see Lumpkin and Johnson (2013).

The drifter–altimeter synthesis combines geostrophic velocity anomalies, as derived from altimetric-mapped sea level anomalies, with a gain coefficient taken from the amplitude of concurrent drifter measurements, with Ekman removed (Niiler et al. 2003), to produce weekly snapshots of absolute geostrophic currents (and absolute dynamic topography) at one-third degree resolution. Essentially, the 19 years of full satellite coverage provide information about the fluctuating fields, while the drifter climatology provides the time-mean component plus an adjustment for the amplitude of the time-varying component. The Ekman component is calculated using the Ralph and Niiler (1999) model with updated coefficients (Niiler 2001) and geostrophic currents in the equatorial band are computed after Lagerloef et al. (1999). This synthesis dataset has been used previously to study interannual current variability in the equatorial (Hormann et al. 2012) and South Atlantic (Lumpkin and Garzoli 2011).

Monthly-mean winds were derived from the 10-yr Quick Scatterometer (QuikSCAT) ocean surface winds dataset, version 04. The dataset covers the time period August 1999–October 2009 and has a half-degree resolution.

3. Results

a. The monsoons as static circulations

Seasonally averaged circulations can show currents and connections that do not actually exist at any point in time—for instance, translating features such as Rossby waves and eddies can appear as continuous flows. However, an initial orientation to the major currents of each monsoon is useful, together with the geography and bathymetry of the Arabian Sea. Figure 1 shows two maps of the surface circulation during the northeast and southwest monsoons from the drifter climatology. Schematics of identified currents after Schott and McCreary (2001) are also shown for comparison.

During the northeast monsoon the NMC flows westward into the basin south of India and curves to the north around 70°E to feed the West Indian Coastal Current (Fig. 1). A major anticyclone, the Lakshadweep eddy (Shetye 1998) appears inshore of this current, off the western tip of India. The drifter climatology shows a branch of the NMC continuing west, as previously found by Molinari et al. (1990), but this is an artifact of the seasonal mean, as will be seen in the monthly fields later. At the western boundary, the Somali Current (SC) flows southward between about 10°N and 3°S, feeding into the eastward SECC. Between 5° and 10°N next to the boundary there is a supermesoscale cyclonic circulation not previously identified [Rossby radius of deformation is about 150 km at these latitudes (Chelton et al. 1998), with seasonal variability no more than ±5%]. It appears to be fed by waters from the NMC, which then exit into the Somali Current and eventually cross the equator. However, this cyclonic circulation and its connectivity to the NMC are also largely artifacts of the seasonal mean and we will look at the evolution of this flow in section 3d. In the north of the basin, there is northward flow across the mouth of the Gulf of Aden (which lies between Somalia and Yemen) and a hint of southward flow off the coast of Oman.

During the southwest monsoon, the circulation is predominantly anticyclonic and considerably stronger than during the northeast monsoon (Fig. 1, lower panel), hence the southwest monsoon prevails in the annual-mean circulation (Schott and McCreary 2001). At the western boundary, the Somali Current flows northward, fed from south of the equator by the East African Coastal Current (EACC). While the Schott and McCreary (2001)

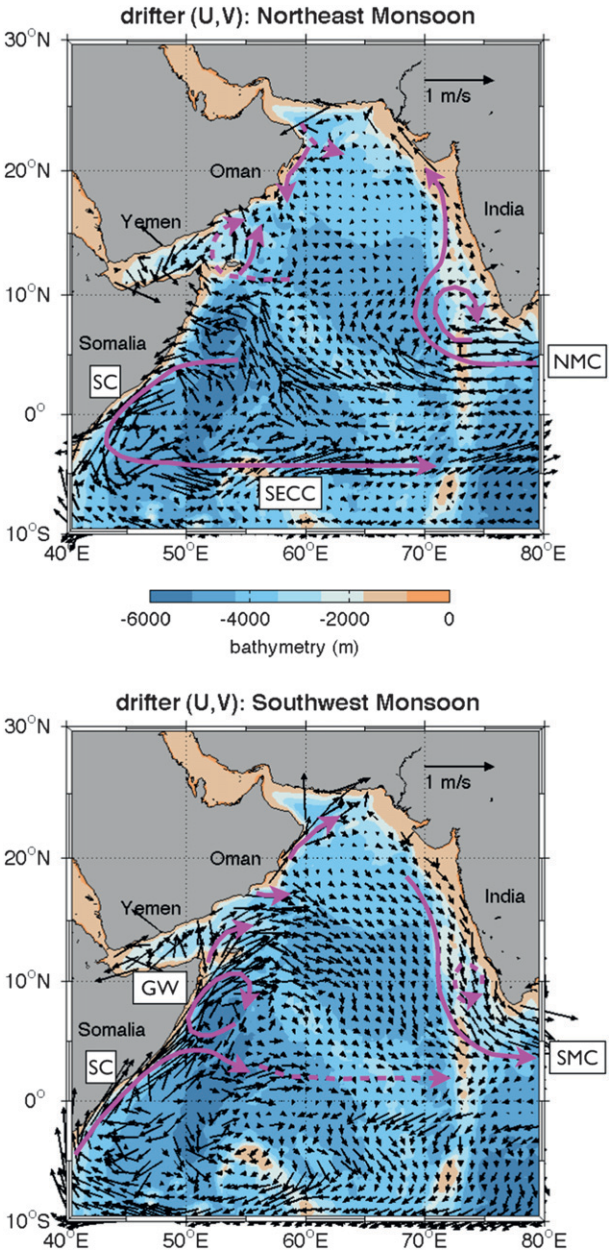

FIG. 1. The circulation of the Arabian Sea (vectors) during the (top) northeast and (bottom) southwest monsoons, from the surface drifter climatology. The northeast (southwest) monsoon is depicted as the currents averaged over the months of December–February (June–August). Magenta arrows are schematics of identified currents after Schott and McCreary (2001). Where the drifter climatology does not reflect the schematic, arrows are dashed. Color shading is bathymetry from 1-min gridded topography for the world (ETOPO1). Landmasses are shaded gray.

schematic shows the boundary current branching into an eastward current at 2° or 3°N, this is not supported by the drifter data. Instead, as we will show later in the geostrophic circulation, this branch loops back across the

equator to feed into the SECC. Farther north, the Somali Current extends across the mouth of the Gulf of Aden and may be connected to northward flow along the Omani coast. A well-known anticyclone, the Great Whirl (GW), appears just off the Somali coast between 5° and 10°N. In the interior, the schematic hints at offshore flow to the east of the Gulf of Aden and the drifter climatology confirms this, showing a strong, broad flow away from the western boundary between 10° and 18°N. Finally, the Southwest Monsoon Current (SMC) flows out of the basin in the east, around the coast of India, in the opposite direction to the NMC.

b. *Monthly evolution of winds, surface currents, and dynamic height*

Monthly-mean fields can provide a description of the evolution of the circulation in the Arabian Sea over the course of a climatological year, beyond treating each monsoon as a static circulation. In this way, we can describe the circulation and its various features more precisely and begin to examine how they may be responding to local and remote forcing. We first present the monthly-mean fields and the basin wide leading modes of variance. Then, in the following sections, we draw attention to several features in particular, which bring us to some new conclusions and some new questions about the monsoon circulation of the Arabian Sea.

The monsoon winds over the Arabian Sea are predominantly northeasterly from November through March and southwesterly from May through September (Fig. 2). During the winter, or northeast monsoon, positive wind stress curl (i.e., upwelling favorable) is dominant over the basin, while during the summer, or southwest monsoon, negative curl dominates. The strongest winds extend off the Horn of Africa and parallel to the coastline of the Arabian Peninsula during June, July, and August and are known as the Findlater jet (Findlater 1969). This jet causes strong positive wind stress curl and oceanic upwelling along the coasts of northern Somalia, Yemen, and Oman during the southwest monsoon, in addition to the negative (downwelling) curl offshore. Winds over the Arabian Sea are weakest in the intermonsoon months of April and October. On the equator, zonal winds are semiannual, with easterlies during the height of the monsoons (January–February and July–August) and westerlies during the intermonsoon months. As a result, equatorial divergence and upwelling does not occur year-round as it does in the Atlantic and Pacific (Schott et al. 2009). Cross-equatorial winds are southerly during the southwest monsoon and northerly during the northeast monsoon.

The monthly evolution of surface currents derived from the drifter climatology is shown in Fig. 3, together with formally estimated errors. A combination of few observations and high variance typically lead to large errors, which are maximal in the west and along the equator. Errors reach over $0.5\,\mathrm{m\,s^{-1}}$ in the Gulf of Aden year-round. During the southwest monsoon, errors over $0.5\,\mathrm{m\,s^{-1}}$ are also found at the mouth of the Gulf of Oman in the northern apex of the basin, and in the southern arm of the southern gyre, which straddles the equator at the western boundary. Elsewhere, errors are typically smaller than $0.2\,\mathrm{m\,s^{-1}}$ and less than $0.05\,\mathrm{m\,s^{-1}}$ in the interior. Clear features of the drifter data are the Wyrtki jets along the equator (Wyrtki 1973): strong ($>1\,\mathrm{m\,s^{-1}}$) eastward flow in April/May and October/November, driven primarily by the semiannual zonal winds (Han et al. 1999; Nagura and McPhaden 2010a). This is a good indication that these data are providing robust semiannual signals, even in regions affected by low data coverage.

Drifter velocities include both the Ekman and geostrophic components of the flow. To elucidate features and their relation to local and remote forcing, it is useful to separate these components. Figure 4 shows the monthly-mean geostrophic currents as derived from the drifter–altimeter synthesis, superimposed on absolute SSH fields. To first order, we expect the differences between Figs. 3 and 4 to be dominated by Ekman velocities set up by the large-scale wind fields in Fig. 2. The leading mode of variance of the Ekman velocities gives an overall sense of how the Ekman flow modifies the geostrophic currents at the surface and is shown in Fig. 5a. This leading mode results from a complex empirical orthogonal function (EOF) analysis on $V(x, t) = u(x, t) + iv(x, t)$, where u and v are the zonal and meridional velocity components, respectively, and $i = \sqrt{-1}$ (e.g., Kundu and Allen 1976; Kaihatu et al. 1998). We choose a complex EOF rather than a harmonic analysis because the vector fields of the eigenmodes can be obtained and the leading circulation pattern more easily visualized. As we would expect, the leading modes for both Ekman and geostrophic velocities correspond to (largely) annual variability. The majority of the variability in the Ekman currents, 68%, is explained by the first EOF, and it corresponds to offshore and southward flow during the southwest monsoon and onshore and northward flow during the northeast monsoon (Fig. 5). To the south of the equator, the Ekman currents are westward during the southwest monsoon and eastward during the northeast monsoon. The strongest Ekman currents are normal to the Somali coast in summer. Overall, the drifter climatology (Fig. 3) generally exhibits stronger offshore/onshore and cross-equatorial flows than the geostrophic flow field (Fig. 4). One example is in the region 0°–5°S, where southward Ekman flow during the southwest

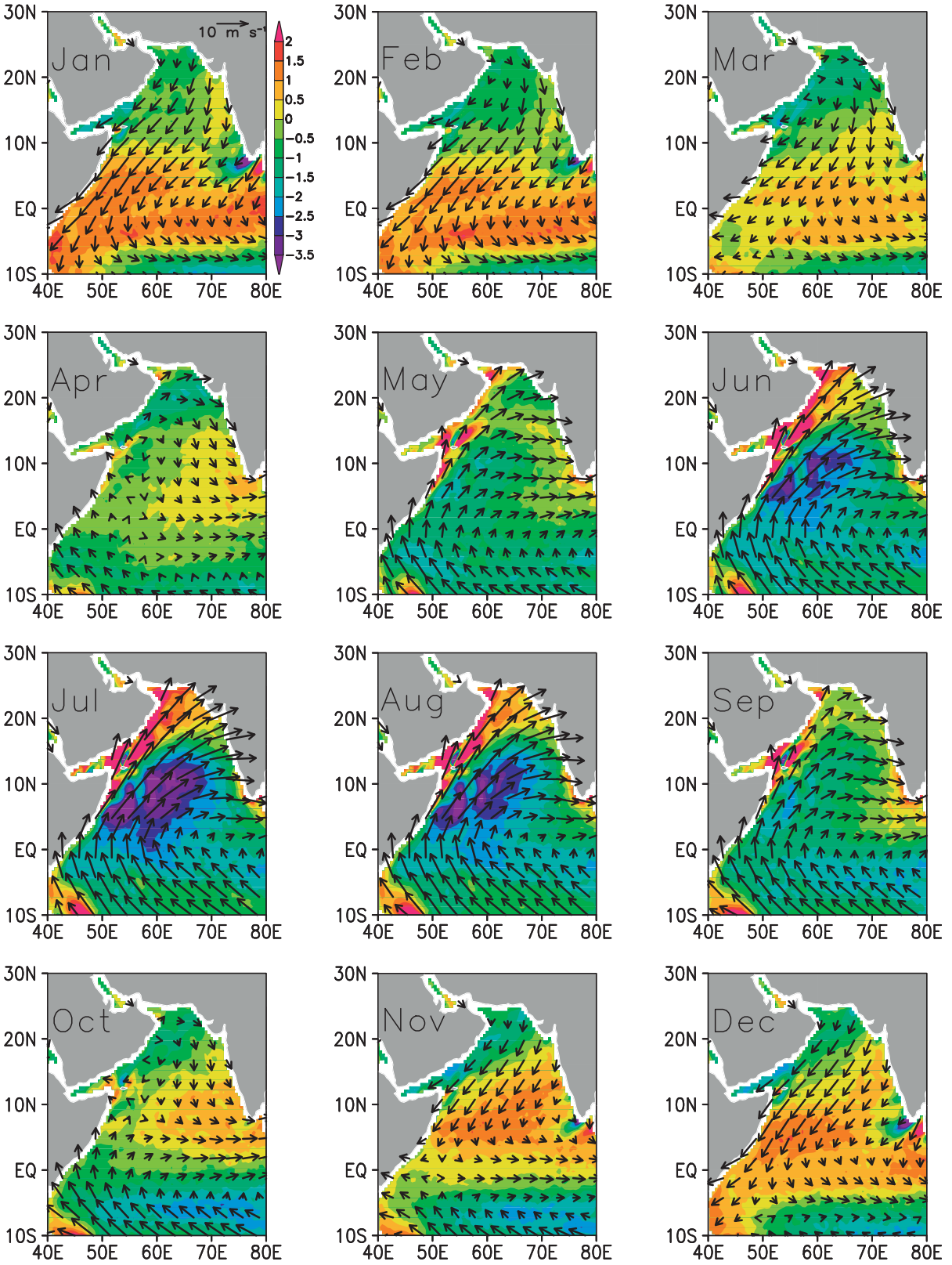

FIG. 2. Monthly winds (vectors; m s^{-1}) and wind stress curl (color shading; N m^{-3}) from QuikSCAT (August 1999–September 2009). Both fields have been fitted to their annual and semiannual harmonics. Landmasses are shaded gray.

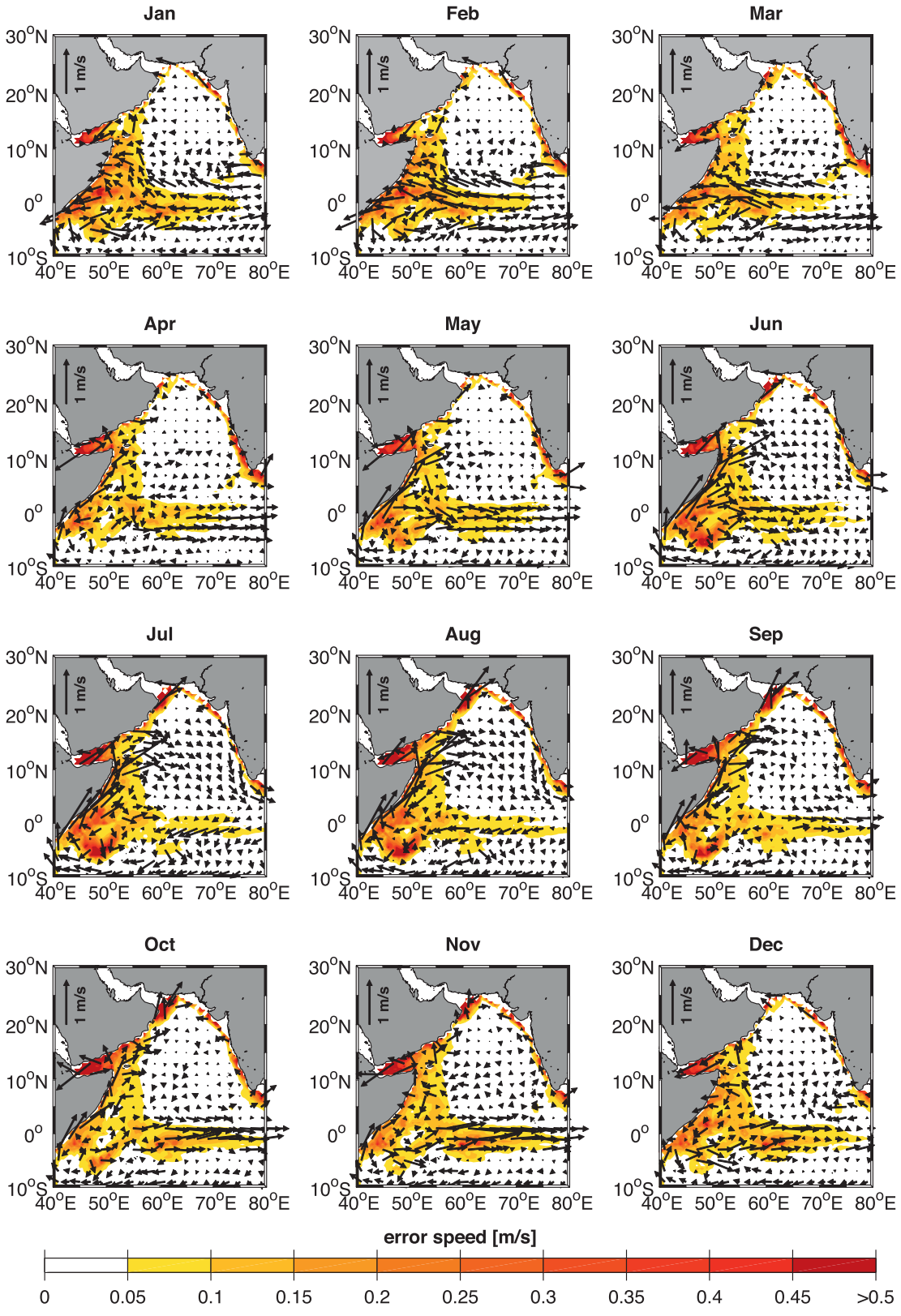

FIG. 3. Monthly-mean absolute, near-surface currents (vectors; m s^{-1}) and formal error speeds (color shading; m s^{-1}) from the drifter climatology. Largest errors occur in the Gulf of Aden, in the region of the southern gyre, and along the equator. Landmasses are shaded gray.

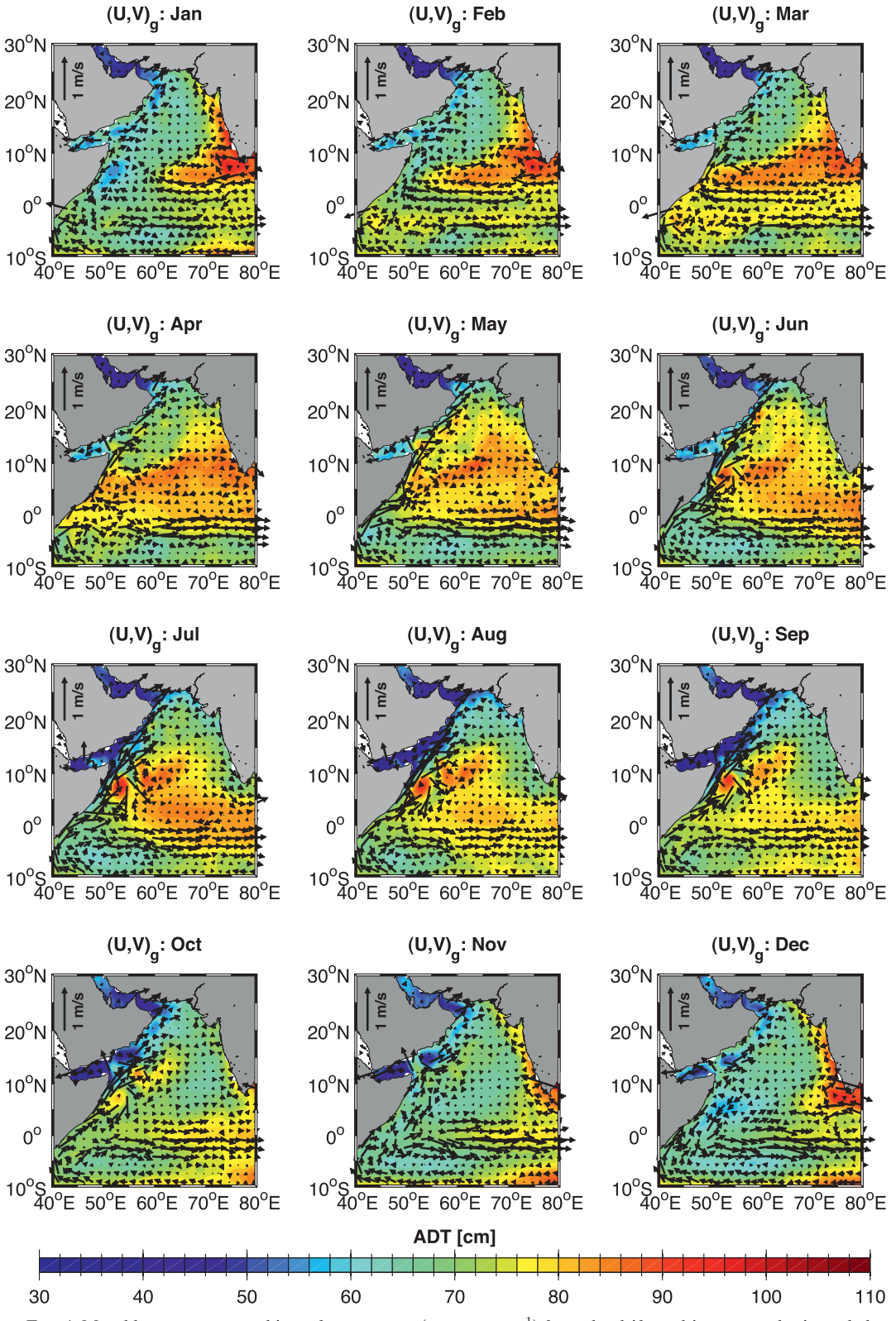

FIG. 4. Monthly-mean geostrophic surface currents (vectors; m s^{-1}) from the drifter–altimeter synthesis, and absolute dynamic topography (ADT; color shading; cm) from Archiving, Validation, and Interpretation of Satellite Oceanographic data (AVISO). Note the early appearance of the GW, or its precursor, in March, and the year-round SECC. Landmasses are shaded gray.

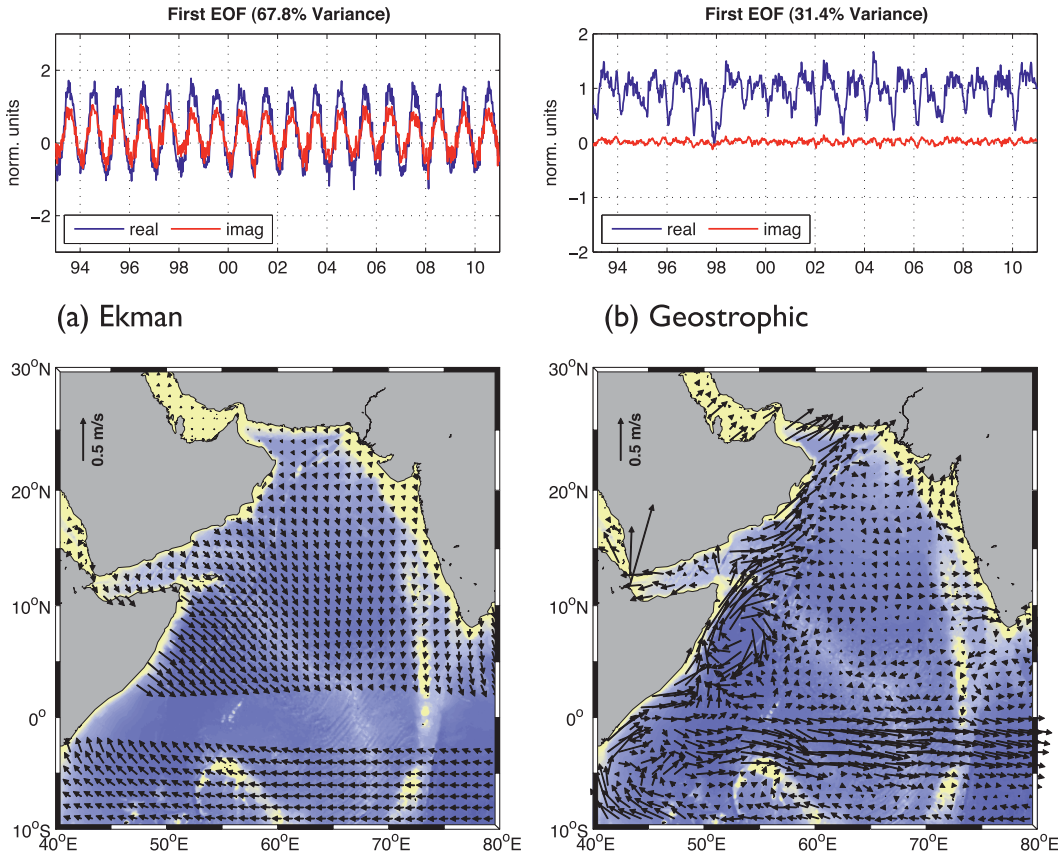

FIG. 5. Structure and phase of the dominant modes of (complex EOFs) variance for (a) Ekman and (b) geostrophic velocities. The top panels show the principal component time series and the bottom panels show the spatial amplitudes of the eigenvectors. Ekman velocities are from NCEP–NCAR reanalysis winds and geostrophic velocities are from the drifter–altimeter synthesis.

monsoon obscures the eastward geostrophic flow of the SECC, as discussed in the following section.

For the geostrophic field, the first EOF (explaining 31% of the variance) features a Great Whirl, northward flow along the entire western boundary, including across the mouth of the Gulf of Aden and along the coast of Oman, and eastward flow just south of the equator in the SECC. The zonal variance is much greater than the meridional variance for this basinwide mode; nevertheless, the SECC flows eastward year-round (Fig. 4) while the meridional Somali Current switches between northward and southward. The NMC and SMC appear in the second EOF, which explains 6.4% of the basinwide variance (not shown).

c. *South Equatorial Counter Current present year-round*

The drifter–altimeter synthesis (Fig. 4) and our EOF analysis show that there is an eastward current between 0° and 5°S year-round. This is the SECC, which was previously thought to be stemmed or even reversed during summer and fall, when there is a component of easterly wind stress south of the equator (Shenoi et al. 1999; Schott and McCreary 2001) (Fig. 2). In fact, southward Ekman currents at the surface obscure the geostrophic circulation south of the equator during the southwest monsoon, which remains eastward throughout the year as a result of a sustained low in SSH centered between 5° and 10°S (Fig. 4). This low is the signature of the Indian Ocean's tropical gyre, bounded in the north by the SECC, to the south by the SEC, and at the western boundary by the EACC.

Figures 6a and 6b show an 18-yr time series of SECC strength and latitudinal position, respectively, together with their annual plus semiannual harmonic. Here, the SECC is defined as the mean zonal geostrophic velocity between 0° and 5°S, 50° and 80°E. Choosing a larger region from the coast at 40°E does not yield significantly different results. The latitudinal position of the SECC is defined by the latitude of the zonal velocity maximum.

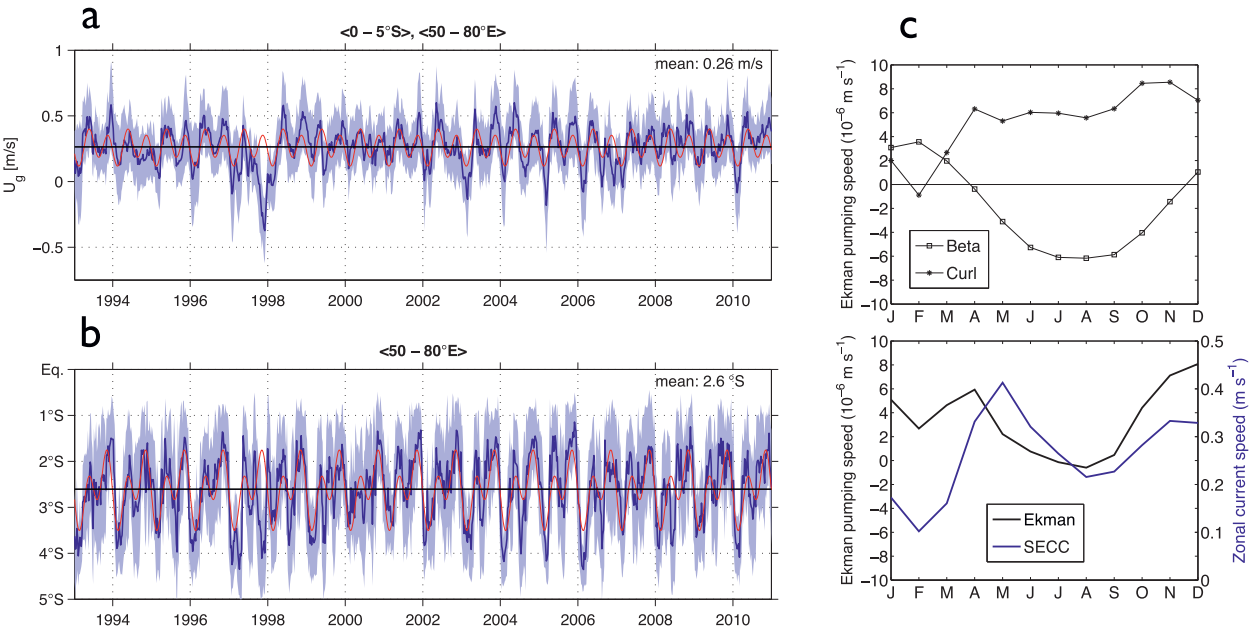

FIG. 6. Time series of (a) the zonal geostrophic velocity U_g and (b) the core position of the SECC, averaged over the longitudinal range 50°–80°E. The leading harmonics (annual and semiannual) are shown in red and shading represents plus or minus one standard deviation. (c) The seasonal cycle of Ekman pumping (from QuikSCAT) over the equatorial gyre (5°–10°S, 50°–80°E) and of the SECC (U_g) are shown. SECC data are from the drifter–altimeter synthesis.

The mean surface velocity of the SECC from this 18-yr time period is $0.26 \pm 0.22\ \mathrm{m\,s^{-1}}$ and its mean position is 2.6° ± 1°S. There are only a handful of events when the currents in the region of the SECC are westward, most notably during the 1997/98 El Niño and positive Indian Ocean dipole event, consistent with Nagura and McPhaden (2010b). The dominant variability is semiannual, with velocity maxima in the intermonsoon months of May and November and minima during the monsoons in February and August. There is a significant correlation (0.7 at zero lag) between the strength and position of the SECC, such that it is shifted to the south when it is weakest, and to the north when it is strongest.

For half the year, the EACC feeds directly into the SECC, without crossing the equator. But from April through September, cross-equatorial winds play a role in causing an overshoot of the EACC (Cane 1980), as can be seen in Fig. 4. The EACC then splits, with a branch continuing northward as the rapidly intensifying Somali Current, while another branch separates from the coast at 3°N and loops back across the equator to continue feeding the SECC. While we might expect a reduction in SECC transport (and by extension its velocity) in correlation with this splitting of its source, the mean SECC velocity is actually strongest at this time. It is weakest in February, when the westward NMC impinges on the equator, weakening the SECC and pushing it to the south (Figs. 4 and 6).

In fact, the semiannual signal in the SECC is predominantly governed by Ekman pumping over the equatorial gyre, which, as Yokio et al. (2008) show, results from both wind stress curl and from the equatorial divergence, or Beta term, of the zonal wind stress, as follows:

$$w_{\mathrm{Ek}} = \frac{1}{\rho f}\,\mathrm{curl}\tau + \frac{\beta\tau_x}{\rho f^2}, \tag{1}$$

where ρ is the density of seawater, f is the Coriolis parameter, β is the meridional gradient of the Coriolis parameter, τ is the wind stress, and τ_x is the zonal component of wind stress. Figure 6c shows that the annual cycles of the curl and Beta terms in Eq. (1) are out of phase (top panel), resulting in a semiannual cycle in Ekman pumping and in the SECC (bottom panel). For instance, during the southwest monsoon from June through September, the easterly component of the strong monsoon winds close to the equator (Fig. 2) causes downwelling over the Southern Hemisphere tropical gyre, opposing the upwelling from the negative curl of the wind stress. Hence, the Beta term causes a minimum in the SECC when the curl is strongest.

The apparent one-month delay between the Ekman pumping and the strength of the SECC in spring (Fig. 6c) is not robust among wind products. We calculated the Ekman pumping using the QuikSCAT data (as shown in

Fig. 2), while Yokio et al. (2008) make the same calculation with four other wind products and find that two give Ekman pumping maxima in May and two in April. However, the SECC could also be influenced by the Wyrtki jets, which are eastward on the equator in May–June and October–November (Wyrtki 1973). Although these jets are predominantly Ekman phenomena, they owe some of their amplitude to semiannual Rossby waves (Nagura and McPhaden 2010a), and it is these that may influence the geostrophic SECC strength.

It is worth briefly mentioning what the drifter data reveal about the so-called southern gyre, a cross-equatorial recirculation found at the western boundary during the southwest monsoon and featured in results from the Indian Ocean Experiment of 1979 (Swallow et al. 1983). Our analysis shows that the southern gyre is not a recirculation but rather a retroflection: its northern arm is formed by the separation of the EACC and its retroflection back across the equator to feed into the SECC (Fig. 4). The drifter climatology (Fig. 3), which shows the total surface flow, indicates that westward Ekman currents south of the equator may give the appearance of a closed southern gyre. These results deserve a little caution owing to large errors in the climatology in this region (7°S, 50°E).

d. The effect of annual Rossby waves on the circulation

The monthly-mean geostrophic currents shown in Fig. 4 reveal that northward flow appears along the length of the western boundary as early as April, together with a weak anticyclone at 6°N, a precursor to the Great Whirl. The early arrival of the Great Whirl was recently noted by Beal and Donohue (2013) in a regional study of SSH data. These observations challenge the concept that the western boundary flow is established after an adjustment of the circulation to the southwest monsoon wind stress curl (e.g., Lighthill 1969). In this case, we would expect a minimum lag on the order of one month between the onset of the wind curl in May–June (Fig. 2) and the appearance of a western boundary current. This is the time scale, according to linear theory, for Rossby waves to propagate from the region of wind curl forcing to the western boundary near the equator (Lighthill 1969). North of 6°N, the theoretical time scale increases by an order of magnitude. Hence, these observations point to a different forcing for the initiation of the northward boundary flow. This is not to say that monsoon winds and wind stress curl do not play the dominant role in forcing the Somali Current once the southwest monsoon sets in, but initial northward flow is clearly established by a different process.

Looking again at Fig. 4, the appearance of northward flow along the boundary in April is coincident with the arrival of an annual high in absolute dynamic topography, centered along 8°N. The exception to this is north of Somalia, where northward flow close to Yemen and Oman occurs year-round. This signal is due to first- and second-mode annual Rossby waves (Brandt et al. 2002), which form part of a waveguide around the northern Indian Ocean as seen in Rao et al. (2010), their Fig. 1b. Shetye (1998) theorizes that the forcing originates during the previous southwest monsoon, when strong, negative wind stress curl triggers a chain of (linear, free) planetary waves which feed back on the initiating region in a predicted time scale of approximately 300 days. This process begins with a westward, downwelling Rossby wave from the wind curl region to the Somali Coast, continues with coastal then equatorial Kelvin waves, and concludes with the propagation of a Kelvin wave around the rim of the Bay of Bengal (Subrahmanyam et al. 2001; Shankar and Shetye 1997), which radiates Rossby waves back into the Arabian Sea from the southern tip of India. (The Kelvin wave does not make it around to the west coast of the Arabian Sea itself, as a result of its rapidly diminishing lateral scale with latitude and the gap in the coastal boundary at the Gulf of Oman). This implies that forcing from the previous southwest monsoon feeds back on the circulation in the Arabian Sea two months ahead of the following monsoon.

We highlight the interplay of remote and local forcing on the circulation in Fig. 7, which shows longitude–time sections of the seasonal cycles of the wind stress curl, SST, and SSH anomalies along 8°N in the Arabian Sea. The annual Rossby wave (SSH high) radiates off the southwest tip of India at 80°E in October/November and propagates westward. The leading edge reaches the west coast in April, so that the offshore gradient of SSH changes sign and the coastal current switches from southward to northward (Figs. 7 and 4). The elevation of the propagated SSH anomaly once it reaches the coast in April (the precursor of the Great Whirl) could result from the reflection of short, coastally trapped Rossby waves (Beal and Donohue 2013). The importance of planetary waves for the coastal currents around the Arabian Sea has been postulated before by McCreary et al. (1993), who saw several examples of remotely forced circulations in their 2.5-layer numerical model. The coastal currents along the west coast of India and the Lakshadweep eddy during the northeast monsoon have been shown to be strongly influenced or dominated by this annual planetary wave process (Shankar and Shetye 1997; McCreary et al. 1993). Moreover, McCreary et al. (1993) suggested that the spring time circulation

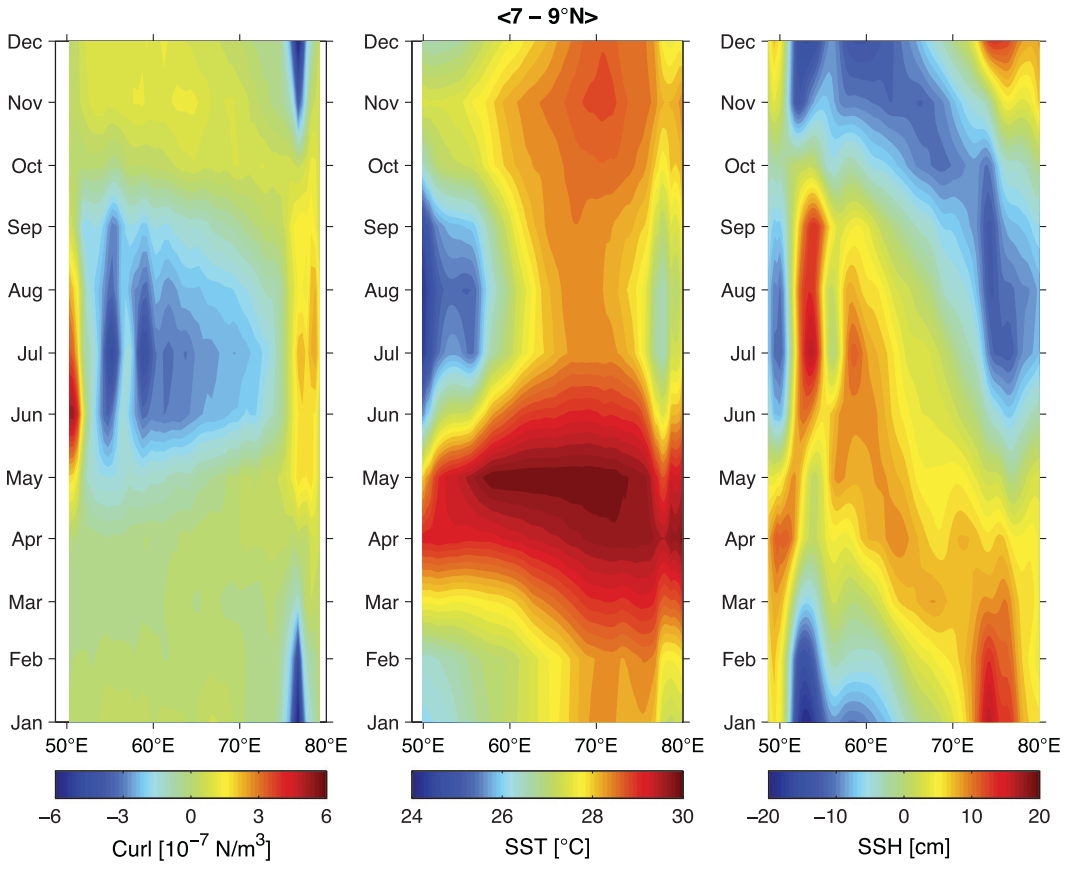

FIG. 7. Longitude–time sections along 8°N (averaged over latitude band 7°–9°N) of annual-averaged wind stress curl ($N\,m^{-3}$) from QuikSCAT (August 1999–September 2009), sea surface temperature (°C) from Group for High Resolution Sea Surface Temperature (GHRSST) (January 1993–December 2011), and sea surface height anomalies from AVISO (January 1993–December 2011).

along the coast of Somalia is influenced by this remote forcing. This is borne out by our study.

The drifter–altimeter synthesis clearly shows that the North Monsoon Current is also strongly influenced by the previous southwest monsoon via the northern Indian Ocean waveguide. In contrast to the static NMC of Fig. 1, the monthly-mean geostrophic circulation (Fig. 4) shows that the NMC gradually extends westward across the basin from December through March, on the southern flank of the Rossby wave high. It does not connect with the supermesoscale cyclone in the west, because the cyclone is gone by the time the NMC reaches the western boundary. In addition to the westward NMC on the southern flank of the Rossby wave high, there is some compensating flow to the east on its northern flank. In this way, the Rossby waves appear to play a role in the initiation of anticyclonic circulation throughout much of the basin, one or two months before the southwest monsoon winds pump in negative vorticity directly (Fig. 7). In April, the Rossby wave and the NMC reach the western boundary where energy is transferred to northward boundary flow, and precursors to the Somali Current and Great Whirl appear, as noted above. These observations lead to an important question: is the feedback limited to spring time, or does it influence the next summer monsoon? In other words, is there some predictability for the strength of the monsoon circulation and its associated SSTs and rainfall, based on the strength of the previous monsoon via this planetary wave feedback? It seems likely that this spinup, or preconditioning, influences the intensity of the ocean's response to the subsequent southwest monsoon winds.

Once the summer monsoon winds set in, the influence of remote forcing on the surface currents is no longer significant. In June–August strong local wind curl obliterates the propagating Rossby wave signal, as seen in Fig. 7. Negative (downwelling) wind curl offshore of the Findlater jet builds positive anomalies in SSH, while positive wind curl inshore builds a negative anomaly along the coast. The steep SSH gradient, which results,

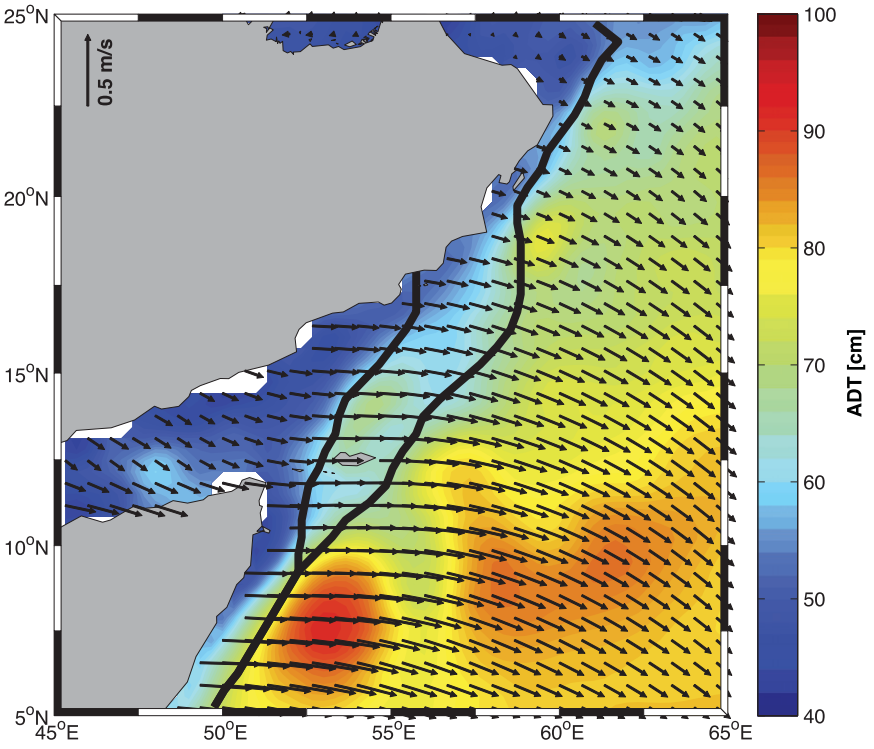

FIG. 8. Ekman currents from the NCEP–NCAR reanalysis winds, as used in the drifter–altimeter synthesis (vectors; m s^{-1}), and absolute dynamic topography from AVISO (color shading; cm), with the two axes of the monsoon jet (wind speed maxima from QuikSCAT data) superposed as thick black lines. All data are averaged over June–August. Landmasses are shaded gray.

drives a strong Somali Current along the boundary. The strongest positive SSH anomaly from June through September is associated with the Great Whirl at 53°E (Beal and Donohue 2013). The positive wind curl, combined with offshore Ekman transports, also drives coastal upwelling and offshore transport of cool waters during the summer, as seen in the evolution of SST (Fig. 7).

e. Broad northward and offshore flow off the Arabian Peninsula

Broad, northward geostrophic flow occurs year-round off the coasts of Yemen and Oman (Fig. 4). There is also strong offshore flow, in both geostrophic and Ekman velocities, at the mouth of the Gulf of Aden during the southwest monsoon. These features have not been discussed much in previous studies and therefore deserve some attention here.

Northward geostrophic flow is associated with a persistent low in SSH along the coast, as seen in Fig. 4. There are hints of quasi-stationary cyclones and an inshore countercurrent during the winter months, but the data resolution is marginal at these latitudes, where the first baroclinic Rossby radius of deformation is only on the order of 50 km (Chelton et al. 1998). The persistent northward geostrophic flow is obscured at the surface by Ekman velocities, which are offshore during the southwest monsoon and onshore during the northeast monsoon, owing to the reversing alongshore winds.

The strongest offshore flow, in both the Ekman and geostrophic circulations, is found during the southwest monsoon over the latitude band from 10° to 18°N (Fig. 1). That is, from the northern flank of the Great Whirl and across the mouth of the Gulf of Aden to the Omani coast. These strong currents are coincident with the axis of the Findlater jet (Fig. 2). The juxtaposition of winds and currents in this region during the height of the southwest monsoon (June–August) is illustrated more closely in Fig. 8. Ekman currents are shown explicitly as vectors, while geostrophic streamlines are shown implicitly via mapped absolute dynamic topography. The Findlater jet is seen to have two axes between 10° and 18°N, as defined by local maxima in wind speed (Fig. 8). The western jet goes through the Socotra Passage and crosses the coast of Oman, while the eastern jet passes to the east of the island of Socotra and continues alongshore toward the Persian Gulf. The Ekman currents flow out of the Gulf of Aden and offshore as a direct response

to these wind jets, while broad, northeastward geostrophic flow is set up along the jet axes by the gradient of SSH, which results from the opposing wind stress curls on either side. The effect of the two wind speed maxima is to cause a local high in SSH north of the island of Socotra, setting up eastward geostrophic flow at the mouth of the Gulf of Aden. Hence, Ekman and geostrophic currents combine during the summer monsoon, such that the surface boundary flow diverts offshore as it crosses the mouth of the Gulf of Aden, as seen in the drifter data in Fig. 1. This results in a broad region of separation of the Somali Current from the coast, much broader than typical western boundary current separations.

4. Conclusions

Drifter and satellite data can resolve the seasonal surface circulation of the Arabian Sea, a region dominated by annually reversing currents driven by the northeast and southwest monsoon winds. These observations address the lack of shipboard and moored observations in the region, which have been nonexistent over the past 10 or 15 years owing to Somali piracy.

We find that the South Equatorial Counter Current flows eastward year-round, fed by the East African Coastal Current and forming the northern flank of the southern Indian Ocean tropical gyre. During the southwest monsoon, the EACC extends across the equator but still feeds into the SECC after separating from the boundary at 3°N and looping back across the equator offshore. Hence, the feature previously known as the southern gyre appears to be a retroflection of the EACC and not a recirculation. At the surface, this circulation is obscured by strong southward Ekman currents. Thus, we argue that the boundary flow in the Arabian Sea during the southwest monsoon should be considered an extension, or overshoot of the EACC up to 3°N, and only north of here is it truly the Somali Current. This may seem like semantics, but it provides larger context. Essentially, the EACC is part of the permanent Southern Hemisphere tropical gyre, overshooting the equator only during the summer owing to strong local winds, while the Somali Current is part of the reversing monsoon circulation around an interior high/low in the Arabian Sea. Of course, the dynamics are more complicated, particularly at the equator, and clearly the gyre boundaries are blurred, with the Southern Hemisphere tropical gyre leaking into the monsoon gyre during the southwest monsoon. But this is a useful framework for understanding the large-scale circulation in the context of the more familiar steady gyres of the Atlantic and Pacific.

During the southwest monsoon, broad northward and offshore flow occurs across the mouth of the Gulf of Aden, coincident with the region of maximum winds and zero wind curl along the axis of the Findlater jet. It is tempting to interpret this feature as a separation and extension of the western boundary current (Somali Current), as would be predicted by linear theory (see Fig. 2). However it is much broader than, for instance, the Kuroshio extension, largely because the zero curl line is alongshore rather than more zonal. Hence, strong offshore flow at the surface appears to be driven by local wind forcing rather than the large-scale wind curl. In addition, the Findlater jet splits into two axes around the island of Socotra forming a local high in SSH at the mouth of the Gulf of Aden, which drives some offshore geostrophic flow. The relation of this flow to the creation of eddies in the Gulf of Aden and to the seasonal pathway of water from the Red Sea exiting the Gulf at depth remain open and interesting questions.

Weak basinwide anticyclonic circulation, a northward boundary flow, and a precursor to the Great Whirl occur in April, two months before the onset of the southwest monsoon winds. This circulation results from the propagation of Rossby and Kelvin waves around the northern Indian Ocean waveguide, which in turn are initiated by strong downwelling wind curl during the previous southwest monsoon. This interesting observation leads to several important questions concerning predictability and feedbacks. Would the southwest monsoon circulation look the same without the planetary wave feedback mechanism? Does it dampen or enhance interannual or decadal variability of the monsoon circulation? Is it possible that an ocean pathway exists through which one monsoon can precondition the next? For the case of a stronger than normal southwest monsoon, there will tend to be stronger downwelling-favorable wind stress curl in the Arabian Sea, resulting in a larger positive sea level anomaly. This sea level anomaly will propagate around the basin and back to the western Arabian Sea by April of the following year, tending to deepen the thermocline anomalously, which could lead to an increase in SST off the coast of Somalia through a reduction in upwelling. The higher than normal SST would then transfer more moisture to the atmosphere, potentially contributing to stronger Indian summer monsoon rainfall (Izumo et al. 2008). The complex balance and coupling between alongshore wind, upwelling, wind curl, Ekman pumping, mechanical mixing, and SST in the western Arabian Sea (Lee et al. 2000; Vecchi et al. 2004) means that these issues deserve further study in a fully-coupled climate model.

Acknowledgments. GF, VH, and RL were funded by NOAA's Climate Program Office and the Atlantic Oceanographic and Meteorological Laboratory. VH was

also supported by the Global Drifter Program, National Oceanic and Atmospheric Administration (NOAA) Grant NA10OAR4320156. Drifter data are available at NOAA's Global Drifter Program (http://www.aoml.noaa.gov/phod/dac). The altimeter products were produced by Segment Sol multimissions d'ALTimétrie, d'Orbitographie et de localisation précise (SSALTO)/Data Unification and Altimeter Combination System (DUACS) and distributed by AVISO (www.aviso.oceanobs.com/duacs), with support from Centre National d'Études Spatiales (CNES). QuikSCAT data are produced by Remote Sensing Systems and sponsored by the National Aeronautics and Space Administration (NASA) Ocean Vector Winds Science Team and are available online (www.remss.com). High-resolution sea surface temperature data were produced by GHRSST (https://www.ghrsst.org/).

REFERENCES

Beal, L. M., and K. A. Donohue, 2013: The Great Whirl: Observations of its seasonal development and interannual variability. *J. Geophys. Res.,* **118,** 1–13, doi:10.1029/2012JC008198.

Brandt, P., M. Dengler, A. Rubino, D. Quadfasel, and F. Schott, 2002: Intraseasonal variability in the southwestern Arabian Sea and its relation to the seasonal circulation. *Deep-Sea Res. II,* **50,** 2129–2141.

Cane, M., 1980: On the dynamics of equatorial currents, with application to the Indian Ocean. *Deep-Sea Res.,* **27A,** 525–544.

Chelton, D. B., R. A. deSzoeke, M. G. Schlax, K. E. Naggar, and N. Siwertz, 1998: Geographical variability of the first baroclinic Rossby radius of deformation. *J. Phys. Oceanogr.,* **28,** 433–460.

Findlater, J., 1969: A major low-level air current near the Indian Ocean during the northern summer. *Quart. J. Roy. Meteor. Soc.,* **95,** 280–362.

Han, W. Q., J. P. McCreary, D. L. T. Anderson, and A. J. Mariano, 1999: Dynamics of the eastern surface jets in the equatorial Indian Ocean. *J. Phys. Oceanogr.,* **29,** 2191–2209.

Hormann, V., R. Lumpkin, and G. R. Foltz, 2012: Interannual North Equatorial Countercurrent variability and its relation to tropical Atlantic climate modes. *J. Geophys. Res.,* **117,** C04035, doi: 10.1029/2011JC007697.

Izumo, T., C. de Boyer Montégut, J.-J. Luo, S. K. Behera, S. Masson, and T. Yamagata, 2008: The role of the western Arabian Sea upwelling in Indian monsoon rainfall variability. *J. Climate,* **21,** 5603–5623.

Kaihatu, J. M., R. A. Handler, G. O. Marmorino, and L. K. Shay, 1998: Empirical orthogonal function analysis of ocean surface currents using complex and real-vector methods. *J. Atmos. Oceanic Technol.,* **15,** 927–941.

Kundu, P. K., and J. S. Allen, 1976: Some three-dimensional characteristics of low-frequency current fluctuations near the oregon coast. *J. Phys. Oceanogr.,* **6,** 181–199.

Lagerloef, G. S. E., G. T. Mitchum, R. B. Lukas, and P. P. Niiler, 1999: Tropical Pacific near-surface currents estimated from altimeter, wind, and drifter data. *J. Geophys. Res.,* **104** (C10), 23 313–23 326.

Lee, C. M., B. H. Jones, K. H. Brink, and A. S. Fischer, 2000: The upper-ocean response to monsoonal forcing in the Arabian Sea: Seasonal and spatial variability. *Deep-Sea Res.,* **47,** 1177–1226.

Lighthill, M. J., 1969: Dynamic response of the Indian Ocean to onset of the southwest monsoon. *Philos. Trans. Roy. Soc. London,* **265,** 45–92.

Lumpkin, R., and S. Garzoli, 2011: Interannual to decadal changes in the western South Atlantic surface circulation. *J. Geophys. Res.,* **116,** C01014, doi:10.1029/2010JC006285.

——, and G. C. Johnson, 2013: Global ocean surface velocities from drifters: Mean, variance, El Niño–Southern Oscillation response, and seasonal cycle. *J. Geophys. Res.,* **118,** 2992–3006, doi:10.1002/jgrc.20210.

——, S. A. Grodsky, L. Centurioni, M.-H. Rio, J. A. Carton, and D. Lee, 2013: Removing spurious low-frequency variability in surface drifter velocities. *J. Atmos. Oceanic Technol.,* **30,** 353–360.

McCreary, J. P., P. K. Kundu, and R. L. Molinari, 1993: A numerical investigation of dynamics, thermodynamics and mixed-layer processes in the Indian Ocean. *Prog. Oceanogr.,* **31,** 181–244.

Molinari, R. L., D. Olson, and G. Reverdin, 1990: Surface current distributions in the tropical Indian Ocean derived from compilations of surface buoy trajectories. *J. Geophys. Res.,* **95** (C5), 7217–7238.

Nagura, M., and M. J. McPhaden, 2010a: Wyrtki jet dynamics: Seasonal variability. *J. Geophys. Res.,* **115,** C07009, doi:10.1029/2009JC005922.

——, and ——, 2010b: Dynamics of zonal current variations associated with the Indian Ocean dipole. *J. Geophys. Res.,* **115,** C11026, doi:10.1029/2010JC006423.

Niiler, P. P., 2001: The world ocean surface circulation. *Ocean Circulation and Climate-Observing and Modeling the Global Ocean,* J. Church, G. Siedler, and J. Gould, Eds., Academic, 193–204.

——, A. S. Sybrandy, K. Bi, P. M. Poulain, and D. Bitterman, 1995: Measurements of the water-following capability of holey-sock and TRISTAR drifters. *Deep-Sea Res. I,* **42,** 1951–1964.

——, N. A. Maximenko, G. G. Panteleev, T. Yamagata, and D. Olson, 2003: Near-surface dynamical structure of the Kuroshio extension. *J. Geophys. Res.,* **108,** C63193, doi:10.1029/2002JC001461.

Pazan, S. E., and P. P. Niiler, 2000: Recovery of near-surface velocity from undrogued drifters. *J. Atmos. Oceanic Technol.,* **18,** 476–489.

Ralph, E. A., and P. P. Niiler, 1999: Wind driven currents in the tropical Pacific. *J. Phys. Oceanogr.,* **29,** 2121–2129.

Rao, R. R., M. G. Kumar, M. Ravichandran, A. Rao, V. Gopalakrishna, and P. Thadathil, 2010: Interannual variability of Kelvin wave propagation in the wave guides of the equatorial Indian Ocean, the coastal Bay of Bengal, and the southeastern Arabian Sea during 1993-2006. *Deep-Sea Res.,* **57,** 1–13.

Schott, F. A., and J. P. McCreary, 2001: The monsoon circulation of the Indian Ocean. *Prog. Oceanogr.,* **51,** 1–123.

——, S.-P. Xie, and J. P. McCreary, 2009: Indian Ocean circulation and climate variability. *Rev. Geophys.,* **47,** RG1002, doi:10.1029/2007RG000245.

Shankar, D., and S. R. Shetye, 1997: On the dynamics of the Lakshadweep high and low in the southeastern Arabian Sea. *J. Geophys. Res.,* **102** (C6), 12 551–12 562.

Shenoi, S. S. C., P. A. K. Saji, and A. M. Almeida, 1999: Near-surface circulation and kinetic energy in the tropical Indian

Ocean derived from lagrangian drifters. *J. Mar. Res.,* **57,** 885–907.

Shetye, S. R., 1998: West Indian Coastal Current and Lakshadweep high/low. *Sadhana,* **23,** 637–665.

Subrahmanyam, B., I. S. Robinson, J. R. Blundell, and P. G. Challenor, 2001: Indian Ocean Rossby waves observed in TOPEX/Poseidon altimeter data and in model simulations. *Int. J. Remote Sens.,* **22,** 141–167.

Swallow, J. C., R. L. Molinari, J. G. Bruce, O. B. Brown, and R. H. Evans, 1983: Development of near-surface flow pattern and water mass distribution in the Somali basin in response to the southwest monsoon of 1979. *J. Phys. Oceanogr.,* **13,** 1398–1415.

Vecchi, G., S.-P. Xie, and A. S. Fischer, 2004: Ocean–atmosphere covariability in the western Arabian Sea. *J. Climate,* **17,** 1213–1224.

Wyrtki, K., 1973: An equatorial jet in the Indian Ocean. *Science,* **181,** 262–264.

Yokio, T., T. Tozuka, and T. Yamagata, 2008: Seasonal variation of the Seychelles dome. *J. Climate,* **21,** 3740–3654.